Silicon (2024) 16:2401–2413
https://doi.org/10.1007/s12633-024-02846-8

RESEARCH

Investigation of the Structural, Elastic, and Radiation Shielding Properties of the SiO_2 –Pb_3O_4–ZnO –Y_2O_3 Glass System

Ali S. Alzahrani[1] · Dalal Abdullah Aloraini[2] · E. A. Abdel Wahab[3] · Kh. S. Shaaban[4]

Received: 1 December 2023 / Accepted: 6 January 2024 / Published online: 13 January 2024

Abstract
This work examined the SiO_2–Pb_3O_4–ZnO–Y_2O_3 glasses mechanical, structural, and radiation shielding features. X-ray diffraction is a powerful technique for investigating the structural properties of these glasses. Experimental results were used to evaluate the mechanical characteristics, and the Makishima and Mackenzie model's semi-empirical approaches were used to investigate the elastic properties. Longitudinal velocity V_L increase from 4935 m/s to 5325 m/s, while transverse velocity V_T increase from 2520 m/s to 2905 m/s. Hardness improved from 4.41 to 8.31 GPa. The behaviour of the elastic moduli at both theoretical and experimental levels is the same. The mass attenuation coefficients (MAC), mean free paths (MFP), tenth & half-value layers (TVL), (HVL), and energy building factors (EBF) were estimated. Overall, higher MAC values were produced by a decrease in ZnO concentration and an increase in Y_2O_3 content. As the concentration of Y_2O_3 increases, the MFP, TVL, and HVL values decrease. Better radiation shielding is provided by lower MFP, TVL, and HVL values. The MFP, TVL, and HVL values are lower in the G 5 sample with the Y_2O_3 contribution (5%, mole). Higher concentrations of Y_2O_3 in glasses with a SiO_2-Pb_3O_4-ZnO-composition were shown to have improved radiation shielding properties.

Keywords Y_2O_3 glasses · Elastic · Radiation shielding · EBF

1 Introduction

Silicate glass has been a focal point in glass science and technology due to its unique properties. This makes it perfect for laboratory glassware, cookware, and even certain high-tech applications like telescope mirrors and premium glassware [1–8]. Researchers continue to explore ways to enhance silicate glass properties, finding new compositions or methods to make it even more resilient, transparent, and adaptable to different environments. This research extends to its applications in various fields like optics, electronics, and medical devices, aiming to push its boundaries further in terms of durability, functionality, and versatility [9–14].

Shielding glasses play a vital role in various critical settings. They offer protection against potentially harmful radiation, intense light or hazardous materials. In medical facilities, these glasses safeguard healthcare workers from exposure to radiation during procedures like X-rays or fluoroscopy. Similarly, in nuclear power plants and industrial environments, they shield workers' eyes from harmful radiation or intense light generated during processes or experiments. The design and materials used in these glasses are tailored to provide the necessary protection without compromising visibility or comfort [15–20]. The structural integrity of radiation shielding materials is crucial for maintaining their effectiveness. Radiation shielding materials are designed to attenuate or absorb ionizing radiation, protecting individuals and equipment from its harmful effects. The fracture strength of glass is indeed pivotal for ensuring its ability to withstand various mechanical stresses. This characteristic becomes particularly important in scenarios where glass is subjected to impacts, or mechanical pressures, as it helps prevent it from breaking or shattering easily. Absolutely, maintaining the integrity of the glass is crucial to

✉ Kh. S. Shaaban
khamies1078@yahoo.com; asalzahrani@tu.edu.sa

[1] Department of Allied Dental Sciences, College of Dentistry, Taif University, P.O. Box 11099, 21944 Taif, Saudi Arabia

[2] Department of Physics, College of Science, Princess Nourah Bint Abdulrahman University, P.O. Box 84428, 11671 Riyadh, Saudi Arabia

[3] Physics Department, Faculty of Science, Al-Azhar University, Assiut P.O 71524, Egypt

[4] Department of Chemistry, Faculty of Science, Al - Azhar University, P.O. 71542, Assiut, Egypt

ensuring its effectiveness as a shield. Any compromise in its structure could significantly reduce its ability to protect against whatever it's shielding from. Absolutely, fracture strength is crucial in radiation shielding materials for several reasons: structural and mechanical strength. The mechanical properties of glasses can vary widely depending on their composition and intended use [21–25].

ZnO – Pb_3O_4- SiO_2 glass is known for its exceptional thermal resistance and optical clarity. Its ability to withstand high temperatures without shattering makes it ideal for various applications, including laboratory glassware, cookware, and glass art. The low coefficient of thermal expansion of ZnO – Pb_3O_4- SiO_2 glass helps it resist cracking or breaking when exposed to rapid temperature changes. Its transparency and durability have made it a preferred choice in industries where these properties are essential. ZnO – Pb_3O_4- SiO_2 glasses have attracted attention due to their large range of structural units and ease of obtaining. Non-destructive ultrasonic techniques were pivotal in understanding the elastic properties of glasses. Researchers use ultrasonic techniques like pulse-echo, acoustic microscopy, and ultrasonic spectroscopy to measure parameters such as velocity waves in glass. By analyzing how these waves propagate and interact within the glass, they can deduce valuable information about the glass's mechanical properties. The ultrasonic velocities, density, and structural data can yield a wealth of information about glass properties. Calculating these parameters can provide a deep understanding of the glass's behavior. The relationship amongst elastic moduli and radiation shielding isn't direct because they are distinct material characteristics with different functionalities [21–25].

Y_2O_3 incorporation can have significant implications, especially in glasses, where alterations in composition often lead to changes in properties. The connection between radiation properties and mechanical strength is crucial, as it can affect the glass's resilience in harsh. This study is part of a broader research effort focused primarily on the impact of Y_2O_3 in this specific context. Understanding the elastic properties of glass is crucial, especially in applications involving radiation shielding. The ability of glass to absorb and attenuate radiation depends on its composition, density, and elastic properties.

2 Materials and Procedure

2.1 Samples Fabrication

The fabrication of glasses samples with varying compositions. The composition as Table 1 indicates different ratios of silicon oxide (SiO_2), lead oxide (Pb_3O_4), zinc oxide (ZnO), and yttrium oxide (Y_2O_3). Sigma Aldrich offers various chemicals that might be used in glass preparation each with a specified purity level, typically 99.9%. These samples were created by using a melt-quenching technique, a common method to produce glasses by melting the raw materials and then rapidly cooling them to solidify. The temperature range of 1150–1200 °C indicates a high-temperature melting point for the glasses involved. The process of melting weighed batches for 3 h with occasional cautious stirring suggests that they achieve a homogeneous melt. Homogeneity in melts is crucial to ensure consistent properties throughout the glasses. Removing stress and thermal strain is crucial to ensure the glass retains its integrity and durability. Therefore, an annealing process in a muffle furnace at 400 °C for all samples is necessary.

Table 1 Chemical compositions Mol %

code	compositions			
	SiO_2	Pb_3O_4	ZnO	Y_2O_3
G 1	60	35	5	0
G 2	60	35	4	1
G 3	60	35	3	2
G 4	60	35	1	4
G 5	60	35	0	5

2.2 Samples Characterization

The influence of varying Y_2O_3 concentrations on various mechanical, optical, thermal, and shielding properties of the borosilicate glass samples was examined through a series of experiments.

XRD is commonly used to explore the structure of glasses, and XRD using the (X'Pert Pro Panalytical diffractometer) with a Si detector and Cu Ka radiation ($\lambda = 1.5406$ Å) and 2 θ= 10 °—90 °, at constant current, 40 mA and constant voltage, 40 mV and with the scanning rate 2°/min.

Archimedes' code is commonly used to measure the density of glass with an accuracy of ± 0.02 g/cm^3 as in the previous works [6, 10].

The pulse-echo method, It's a common technique to quantity the (longitudinal velocity V_L, and transverse velocity V_T) of glasses by (KARL DEUTSCH Echograph model 1085) with an accuracy of $\pm$ 10 m/s. The mechanical factor evaluation formulae are displayed in Table 2. The PSD/Phy-X [26] program utilizes theoretical models to approximation the radiation shielding constraints of the studied glasses at different gamma-ray energies.

Table 2 The mechanical factor evaluation formulae

Eq. No	Parameter	Equation
1	Longitudinal waves	$L = \rho v_l^2$
2	Transverse waves,	$G = \rho v_t^2$
3	Young's modulus	$Y = (1+\sigma)2G$
4	Bulk modulus	$K = L - \left(\frac{4}{3}\right)G$
5	Micro-Hardness	$\mathrm{H} = \frac{(1-2\sigma)\mathrm{Y}}{6(1+\sigma)}$
6	Debye temperature	$\theta_D = \frac{h}{k}\left(\frac{9N}{4\pi V_m}\right)^{\frac{1}{3}} M_s$
7	Average velocities	$M_s = \frac{1}{3}\left(\left(\frac{1}{v_l^3}\right) + \left(\frac{2}{v_t^3}\right)\right)^{-\frac{1}{3}}$
8	Thermal Expansion	$\alpha_{P=23.2(v_L - 0.57457)}$
9	Molar volume of oxygen	$V_o = \left(\frac{M}{\rho}\right)\left(\frac{1}{\sum xini}\right)$,
10	Packing density of oxygen	$OPD = \left(\frac{1000\,C}{Vm}\right)\left(\frac{Mol}{L}\right)$.
11	Dissociation energy	$Gi = \left(\frac{1}{V_m}\right)\sum_i GiXi$
12	Packing density	$V_i = \left(\frac{3\pi}{4}\right)NA\{m\mathrm{R}_{\mathrm{m}}^3 + n\mathrm{R}_{\mathrm{i}}^3\}\left(\frac{m^3}{mol}\right)$
13	acoustic impedance	$Z = V_l\rho$

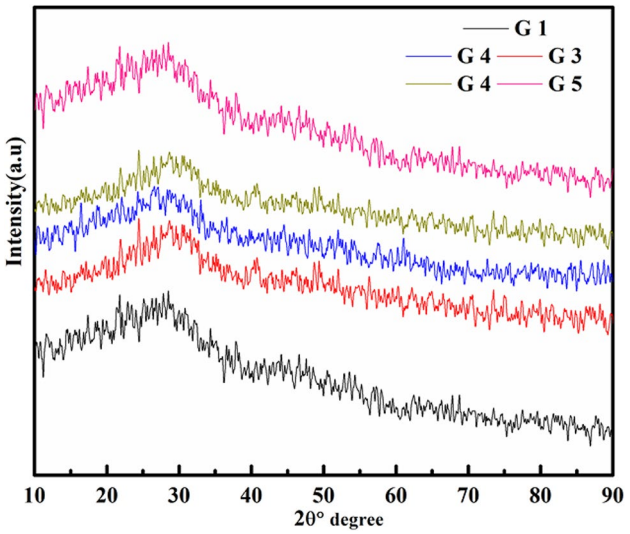

Fig. 1 XRD of SiO_2–Pb_3O_4–ZnO–Y_2O_3 glasses

3 Results and Discussion

3.1 XRD Characteristic

XRD pattern within a specific angular range ($10° \leq \theta \leq 90°$) of (Y^{3+}) co-doped zinc lead silicate samples are displayed in Fig. 1. The lack of sharp diffraction peaks and the presence of broad hump around 23°-30° indicate that the samples are amorphous in nature rather than crystalline. This characteristic broad hump around 23°-30° suggests an amorphous structure in glass samples. The presence of halos at 23°-30° indicates a particular characteristic of these glasses [27–30].

3.2 Physical Parameters

The glass densities (ρ) differed, ranging from 5.91 gcm^{-3} for G1 to 6.97 gcm^{-3} for G5. (ρ) of a glass is influenced by its structure, so (Y_2O_3) is replacing (ZnO) within a glass structure and (Y_2O_3) has a higher molecular mass (225.81 g/mol) than ZnO (81.389 g/mol), which could lead to a small increment in the overall (ρ) [31–35]. Additionally, the molar volume decreased as more Y_2O_3 was added to the glass structure. This might have played a role in the observed variations in glass (ρ). Since density is concerned with the spatial distribution of ions in the structure, (V_m) provides a better explanation for the glass structure than density. There is an inverse correlation amongst the (ρ) and computed (V_m) of the mentioned samples. Typically, when (ρ) increases, (V_m) tends to decrease and vice versa. The decreased in (V_m) might suggest the presence of fewer void spaces or lower intermolecular gaps within the glasses, causing higher (ρ). Figure 2 illustrates the (ρ), and (V_m) of the samples [31–35].

The presenting of Y_2O_3 content caused an increment in the packing density (*OPD*) of the glass system from 55.92 to 66.72 while the V_o decreases from 17.88 to 14.99, indicating a trend toward closer glass structure [36–40]. The (*OPD*) of a glass system increases; it suggests that the atoms or molecules within the structure are arranging themselves

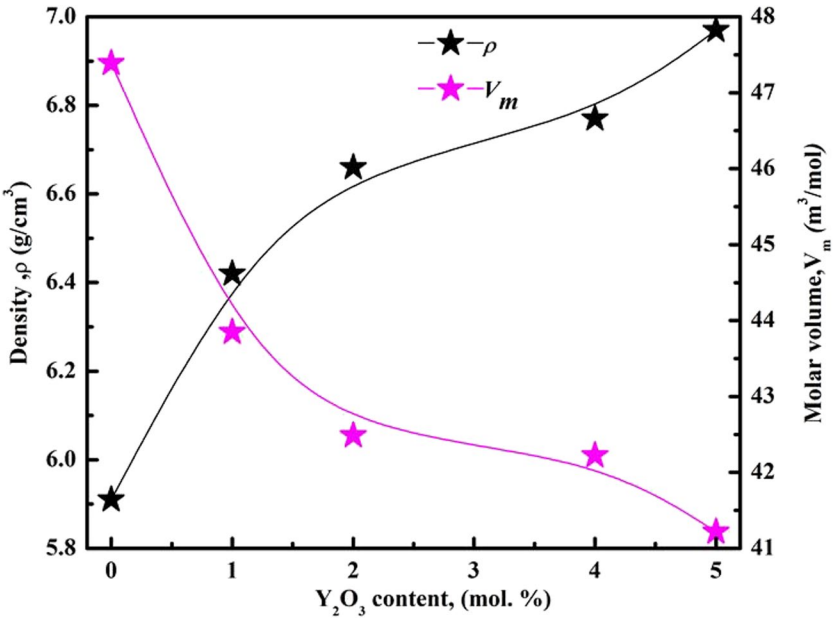

Fig. 2 Density (ρ) &molar volume (V_m) of fabricated glasses

more closely together. In this case, the addition of Y_2O_3 content facilitates this change, indicating a shift toward a more closely packed arrangement of the atoms in the glass structure. This alteration could have various implications for the properties and behavior of the glass [36–40]. Consequently, the involvement of Y^{3+} ions as network modifiers via BO formation is confirmed by the combined decrease in V_o and rise in (*OPD*). The decrease in V_o typically suggests increased (*OPD*) efficiency or a reduction in available space within the structure, while an increment in partial (ρ), could indicate an increment in the mass of a substance per unit volume. Figure 3 illustrates the (*OPD*), and (V_o) of the glasses.

3.3 Mechanical Characteristics

Furthermore, the compositional dependence of density (ρ), (longitudinal velocity V_L, and transverse velocity V_T), and elastic moduli (bulk modulus: *K*, Young's modulus: *Y*, longitudinal modulus: *L*, and transverse modulus: *G*) of all the glass samples are shown in Figs. 4 and 5 [4, 41–47], these data are also found in the studied glasses $35Pb_3O_4 - 60SiO_2 - xY_2O_3 - (5\text{-}x)$ ZnO, ($0 \leq x \leq 5$ mol %). V_L increase from 4935 m/s to 5325 m/s, while V_T increase from 2520 m/s to 2905 m/s. typically, when Y_2O_3 is added to a glass, it can enhance the ultrasonic velocities

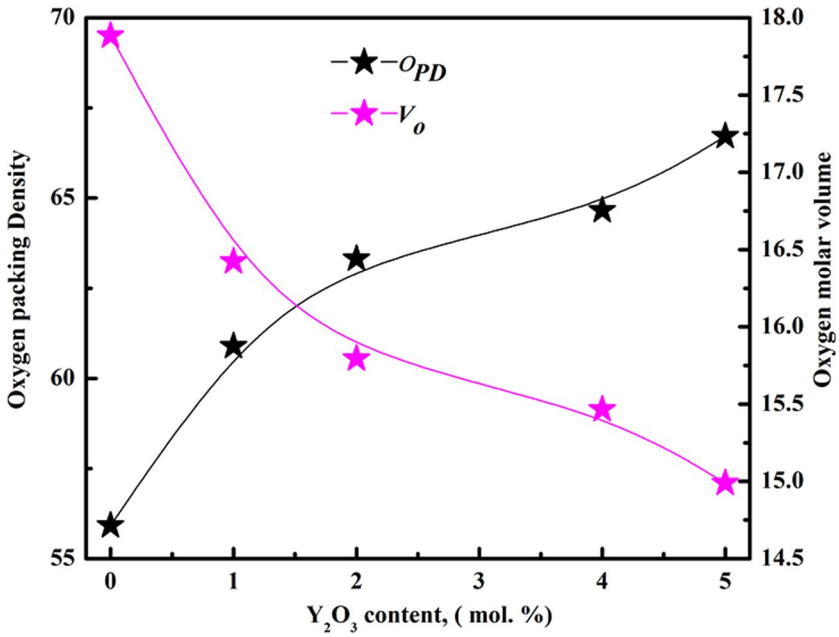

Fig. 3 (*OPD*) & (V_o) versus Y_2O_3 content

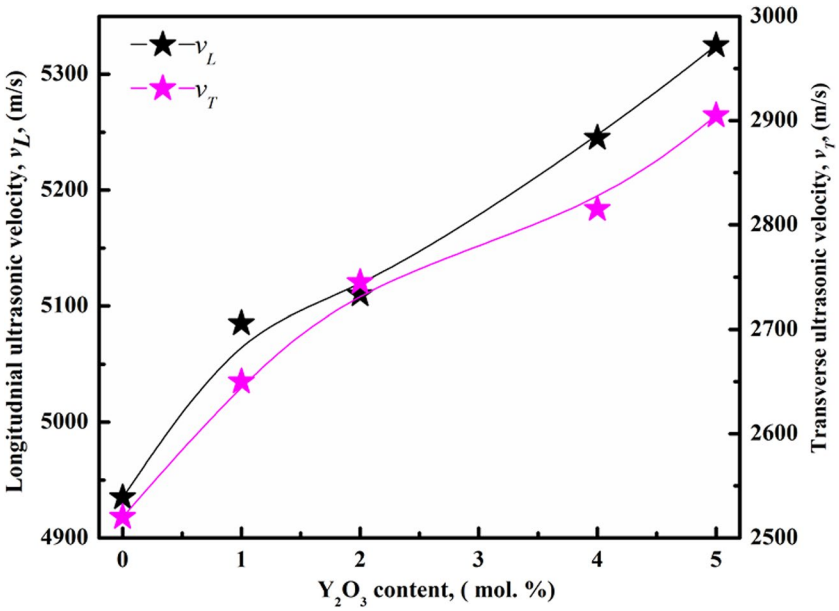

Fig. 4 (V_L) & (V_T), versus Y_2O_3 content

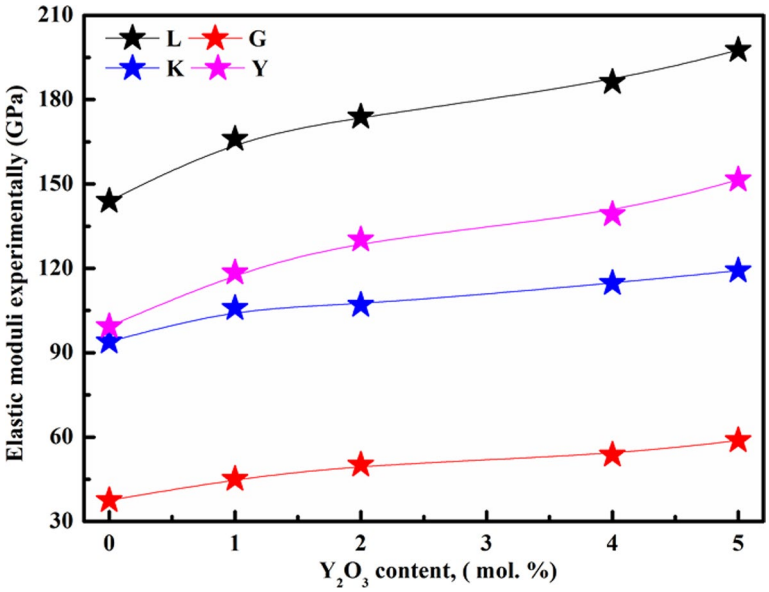

Fig. 5 Experimental elastic moduli versus Y_2O_3 content

and its mechanical properties due to its ability to modify the microstructure and influence the elastic behavior of the glass system. The increase in (longitudinal V_L and shear V_T) with an increase in Y_2O_3 mol % is often associated with changes in the glass density, and stiffness. Moreover, the elastic moduli tend to increment as the Y_2O_3 mol % increments. This is due to Y_2O_3 reinforcing the glass matrix, resulting in improved stiffness and resistance to deformation. As a result, the material becomes stiffer and less prone to elastic deformation. The elastic moduli are correlated with ultrasonic wave velocities. This correlation suggests a relationship between the material's bond types and its mechanical properties. For instance, glasses with stronger or more rigid bonds between atoms might exhibit higher elastic moduli and higher ultrasonic wave velocities compared to a glass with weaker or more flexible bonds. In our studying the single bond strength of Y–O (50 kcals) is greater than Zn–O (36 kcals) [48].

Figure 5 displays the elastic moduli (L, K, G, and Y) of the G1–G5 samples. With the adding of Y_2O_3 at varying mol%, the values of Y increased from 99.35 to 151.51 GPa, suggesting an increase in matrix stiffness. With successive additions of Y_2O_3, the bulk modulus similarly increased, rising from 93.89 to 119.21 GPa. The glasses' L values (143.93–197.64 GPa) were higher than their corresponding G values (37.53–58.82 GPa), suggesting that they are more

Table 3 Mechanical aspects information

parameters	G1	G2	G3	G4	G5
V_L	4935	5085	5110	5245	5325
V_S	2520	2650	2745	2815	2905
L	143.9	166.0	173.9	186.2	197.6
G	37.5	45.1	50.2	53.6	58.8
K	93.9	105.9	107.0	114.7	119.2
Y	99.4	118.4	130.2	139.2	151.5
V_o	17.9	16.4	15.8	15.5	15.0
OPD	55.9	60.9	63.3	64.7	66.7
α_P	114478.67	117958.67	118538.67	121670.67	123526.67
H	4.41	5.60	6.78	7.24	8.31
θ_D	320.2	345.8	362.1	373.8	389.3
M_s	1957.6	2055.9	2125.2	2179.5	2246.5
$Z*10^{-7}$	1.5	1.7	1.83	1.91	2.02

able to tolerate longitudinal stress than shear stress and that they are more easily bent than extended.

Generally, Y_2O_3 in glass can enhance its hardness properties; it can improve the mechanical properties and increase microhardness due to its ability to strengthen the glass. Therefore, microhardness (H), increase from 4.41 GPa, to 8.31 GPa. The Debye temperature is a measure of the average vibrational energy in a solid material. The (θ_D) increase with the addition of Y_2O_3 from 320.2 to 389.3 due: increase the rigidity or stiffness of the glass matrix. Ultimately, the increment in the (θ_D) with the addition of Y_2O_3 in a glass system is a complex phenomenon influenced by multiple factors related to the structural and compositional changes induced by the addition of Y_2O_3 [4, 41–47].

Acoustic impedance (Z) is a quantity of how much confrontation a glass suggestions to the transmission of sound waves. In this case, the increment in the quantity of Y_2O_3 led to an increase in the (Z) of the glass from 1.5×10^{-7} to 2.02×10^{-7}. This increase is due to variations in the density, (V_L), and elastic properties. These changes collectively contribute to an increment in the (Z). Y_2O_3 can influence the thermal expansion (α_P) properties of glass. The (α_P) increases from 114,478.67 to123526.67. This increase is due to changes in the density, (V_L), and elastic properties caused by the addition of Y_2O_3 [4, 41–47]. Table 3 regarding the mechanical properties of fabricated glass samples, velocities, elasticity, hardness, or any other related information's.

3.4 Makishima–Mackenzie's Model (MMM) for Elastic Moduli [49, 50]

Makishima and Mackenzie have developed models that relate to the packing density (V_i) and dissociation energy (Gi) of glasses. The equations for evaluating elastic moduli as (MMM) are presented in Table 4. The change in (V_i) indicates a structural variation due to the presence of Y_2O_3. As the Y_2O_3 component was added, the (V_i) of the glass system increased from 0.385 to 0.4633, and (Gi) increased from 014.42 to 14.81, indicated that the glass structure is getting closer together. Figure 6 displays (V_i) and (Gi) of the G1–G5 glasses. A higher (V_i) typically leads to improved mechanical properties, including compressive strength. This is because a denser arrangement of particles allows for better load distribution and more efficient resistance against compressive forces. With fewer voids or spaces, there's less opportunity for deformation or failure under compression, leading to increased strength. Therefore, with an increase of Y_2O_3 the elastic values based on MMM increased as follow: (Y_{th}) increased from 46.41 to 57.77 GPa,

Table 4 The equations for evaluating elastic moduli as (MMM)

Eq. No	Parameter	Equation
14	Dissociation energy	$Gi = (\frac{1}{V_m})\sum_i GiXi$
15	Packing density	$V_i = \left(\frac{3\pi}{4}\right)NA\{m\mathrm{R}_m^3 + n\,\mathrm{R}_i^3\}(\frac{m^3}{mol})$
16	Longitudinal waves	$L_{th} = K_{th} + \frac{4G_{th}}{3}$
17	Transverse waves,	$G_{th} = \frac{3K_{th}}{10.2V_i - 1}$
18	Young's modulus	$Y_{th} = 8.36V_iG_i$
19	Bulk modulus	$K_{th} = 10V_i^2G_i$

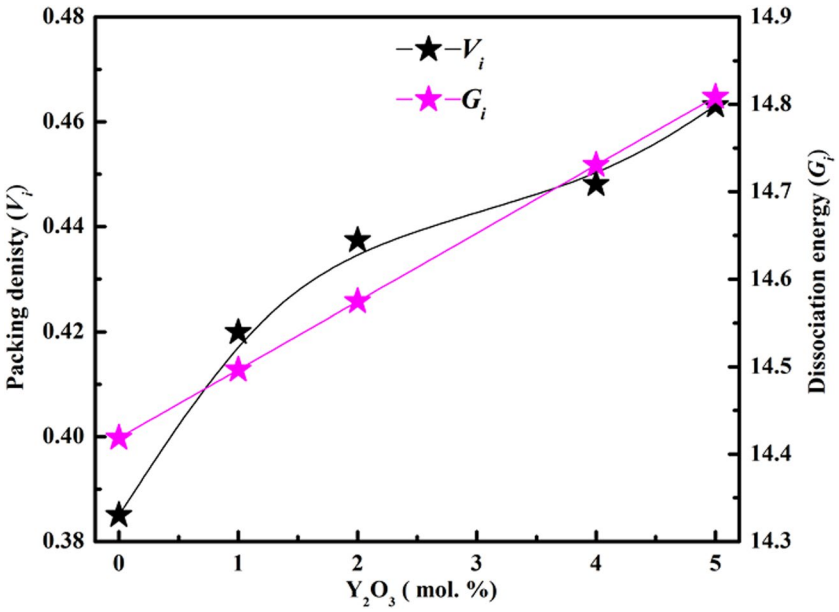

Fig. 6 (V_i) and (Gi) of the G1–G5 glasses

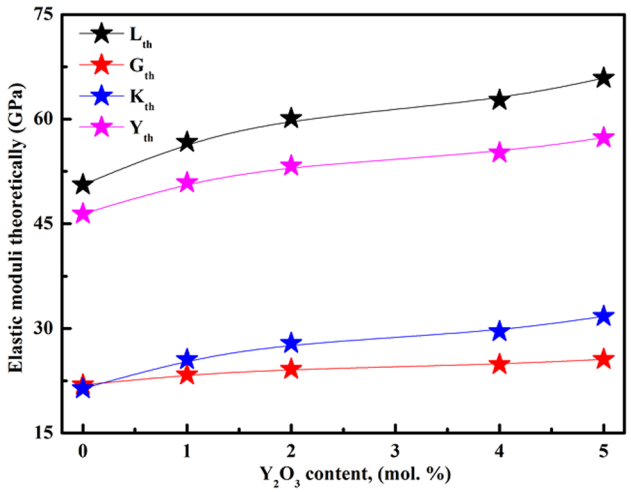

Fig. 7 Theoretically elastic moduli versus Y_2O_3 content

Table 5 values of (V_i), (Gi), and theoretically values of elastic moduli based on MMM

parameters	G1	G2	G3	G4	G5
V_i	0.385	0.420	0.437	0.448	0.463
G_i	14.42	14.50	14.57	14.73	14.81
L_{th}	50.58	56.71	60.10	62.72	65.88
G_{th}	21.91	23.36	24.17	24.85	25.59
K_{th}	21.37	25.56	27.88	29.58	31.77
Y_{th}	46.41	50.89	53.29	55.19	57.34

suggesting an increase in matrix stiffness. With successive additions of Y_2O_3, (K_{th}) similarly increased, rising from 21.37 to 31.77 GPa. The glasses' (G_{th}) values (21.91–25.59 GPa) and (G_{th}) values (50.58–65.88 GPa). Figure 7 and Table 5 displays elastic moduli as (MMM) of the G1–G5 glasses. The behaviour of the elastic moduli at both theoretical and experimental levels is the same [45–47].

3.5 Radiation Shielding Studies

Figure 8 illustrating the Mass Attenuation Coefficients (MACs) of fabricated sample glasses evaluated using the Phy-x code. MAC is essential in understanding how to attenuate or reduce the strength of radiation as it permits through these glasses [51–62]. There is a clear trend that shows that when photon energy (E) increases, the MAC values decline. However, the chemical composition of glass samples affects MAC values. The maximum MAC values are observed in the low (E) region. The main approach that photons interact with matter at low energy ($E < 0.5$ MeV) is through the photoelectric effect (PE). Table 6 and Fig. 8 show that MAC values decrease significantly at 0.15 MeV. This rapid decline is explained by the (PE) in the low (E) zone. In the low (E) region, the photons often interact with glass in ways that involve either whole preoccupation or noteworthy loss of their (E). After 0.15 MeV, it's evident that the MAC values decline more slowly as (E) increases. After this energy limit, Compton scattering dominates, and in this specific region, the Compton scattering cross section varies with respect to (Z) and (E). Overall, higher MAC values were produced by a decrease in ZnO concentration and a rise in Y_2O_3 [51–62].

Figures 9, 10 and 11 show the HVL, TVL and MFP values, which are essential factors for evaluating the material's radiation shielding efficacy. Glass densities and MAC

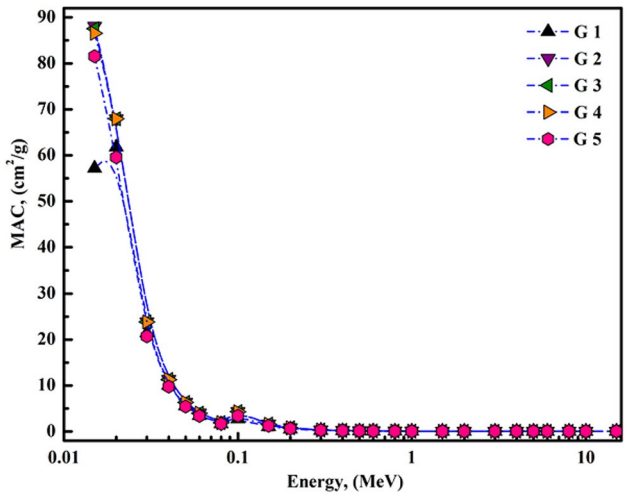

Fig. 8 MAC of fabricated samples

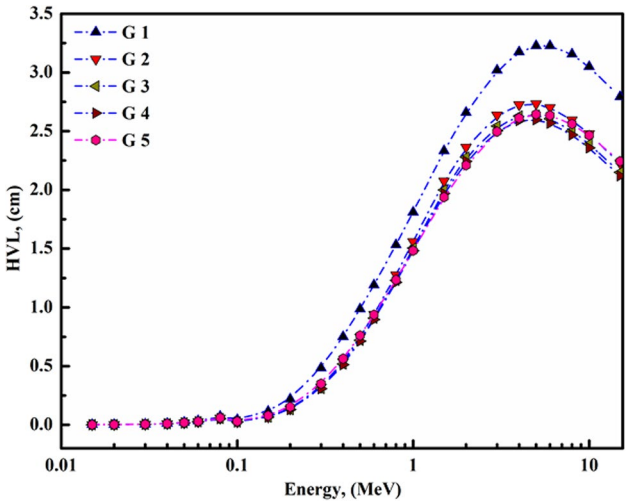

Fig. 9 HVL of fabricated samples

Table 6 MAC (cm^2/g) values of the fabricated glasses

E	G1	G2	G3	G4	G5
0.015	57.188	88.019	87.527	86.559	81.555
0.02	61.785	67.926	67.925	67.924	59.563
0.03	21.423	23.832	23.829	23.824	20.719
0.04	10.021	11.295	11.293	11.287	9.759
0.05	5.556	6.336	6.334	6.329	5.452
0.06	3.442	3.966	3.964	3.959	3.404
0.08	1.648	1.926	1.925	1.922	1.652
0.1	2.741	4.333	4.316	4.281	3.418
0.15	1.023	1.591	1.584	1.572	1.268
0.2	0.532	0.801	0.798	0.792	0.649
0.3	0.242	0.336	0.335	0.333	0.284
0.4	0.156	0.201	0.201	0.200	0.176
0.5	0.119	0.145	0.144	0.144	0.130
0.6	0.098	0.115	0.115	0.114	0.106
0.8	0.077	0.085	0.084	0.084	0.080
1	0.065	0.069	0.069	0.069	0.067
1.5	0.050	0.052	0.052	0.052	0.051
2	0.044	0.046	0.046	0.046	0.045
3	0.039	0.041	0.041	0.041	0.040
4	0.037	0.040	0.040	0.040	0.038
5	0.036	0.040	0.039	0.039	0.038
6	0.036	0.040	0.040	0.040	0.038
8	0.037	0.042	0.042	0.041	0.039
10	0.038	0.044	0.044	0.043	0.040
15	0.042	0.049	0.048	0.048	0.044

values can be used to determine MFP, TVL and HVL values as:

$$HVL = \frac{0.693}{MAC} \tag{20}$$

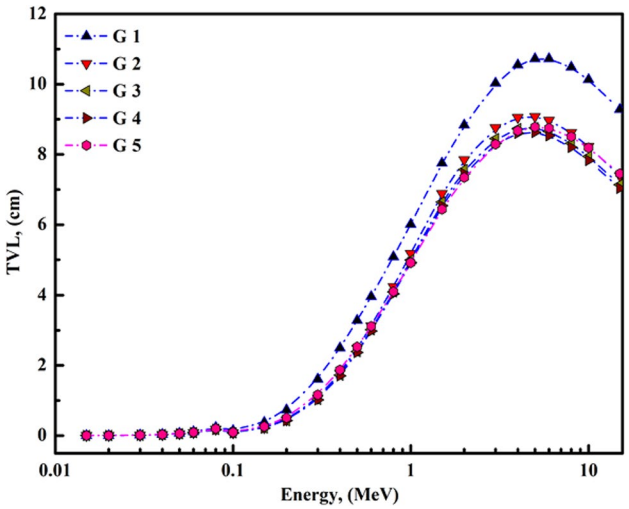

Fig. 10 TVL of fabricated samples

$$TVL = \frac{2.303}{MAC} \tag{21}$$

$$MFP = \frac{1}{MAC} \tag{22}$$

The current glass sample has the lowest MFP, TVL, and HVL values across all (E). As the concentration of Y_2O_3 increases, the MFP, TVL, and HVL values decrease. Better radiation shielding is provided by lower MFP, TVL, and HVL values. The MFP, TVL, and HVL values are lower in the G 5 sample with the Y_2O_3 contribution (5%, mole). The efficiency of the radiation shielding is increased by Y_2O_3's contribution to the proposed glass structure. The inclusion of Y_2O_3 in the glass structure enhances the effectiveness

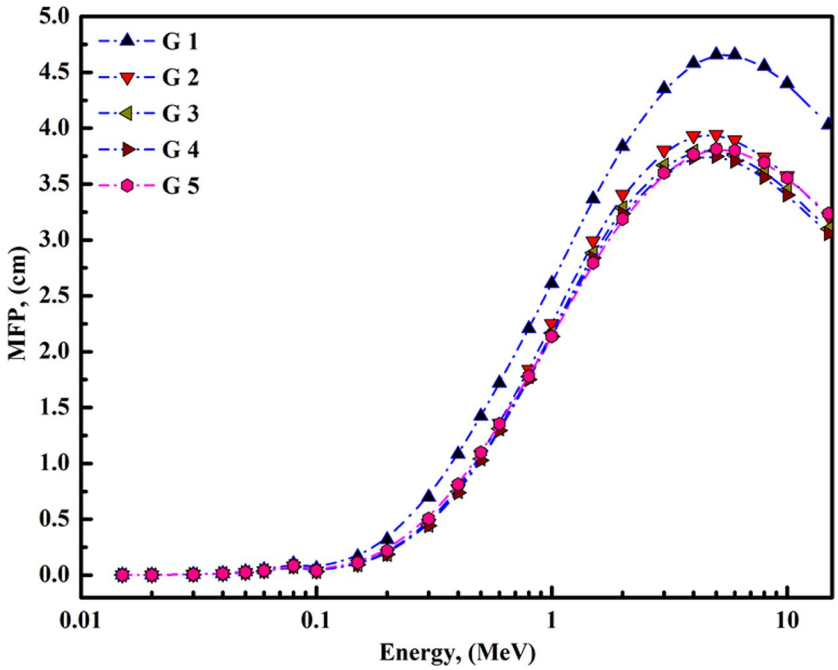

Fig. 11 MFP of fabricated samples

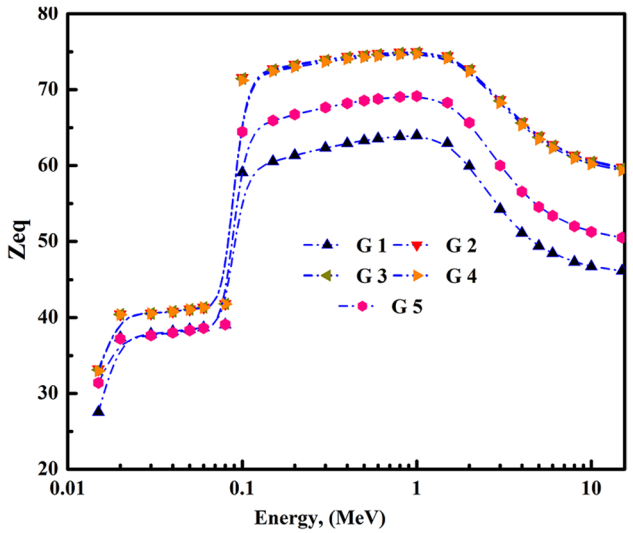

Fig. 12 Zeq of fabricated samples

of the radiation shielding. This improvement is due to the alteration of the current glass properties caused by the addition of Y_2O_3. It could be altering the interactions of radiation with the glasses, resulting in reduced MFP, TVL, and HVL values [63–71].

The equivalent atomic number Zeq must be calculated before beginning the GP fitting computation sequence. The Zeq provides the (Z) of a pure element with photon scattering and accumulation characteristics comparable to those of the composite materials. The energy variation of Zeq for the current glass samples is displayed in Fig. 12. In overall, the glasses with denser materials and higher Y_2O_3 content had larger Zeq at each (E), ranging from 27.55 to 74.99. The minimum and maximum atomic numbers of the constituent elements in a composite material are known to cause variations in the Zeq [63–71].

In the (E) range of 0.015–15 MeV and 0.5–40 mfp, the energy building factors (EBF) of the glasses under investigation were presented in Fig. 12. In lower (E) ranges the EBF tends to be higher. This is because lower-energy radiation is more easily absorbed and tends to interact more frequently with the shielding material, leading to a higher buildup factor. This occurrence may be explained by the statement that photons in this region either lose a substantial amount of energy or are completely absorbed. The (PE), which predominates at lower (E), is the primary cause of this. It is interesting to observe that the quantity of these increases correlates with the oxide concentration in the glass composite sample. The EBF values begin decreasing after 1 MeV. The pair production process operates effectively in this (E), region. Photons significantly lose energy or disappear just like in the (PE). Secondary scattering and photon strengthening can both happen, depending on the composition of the sample. In all samples, EBF values generally trend to decline in the high (E), zone. Figure 13 illustrates that EBF values rise with increasing penetration depth. The smallest EBF values, corresponding to high and low photon energies, are observed in G2, G3, G4 &G5 samples [63–71].

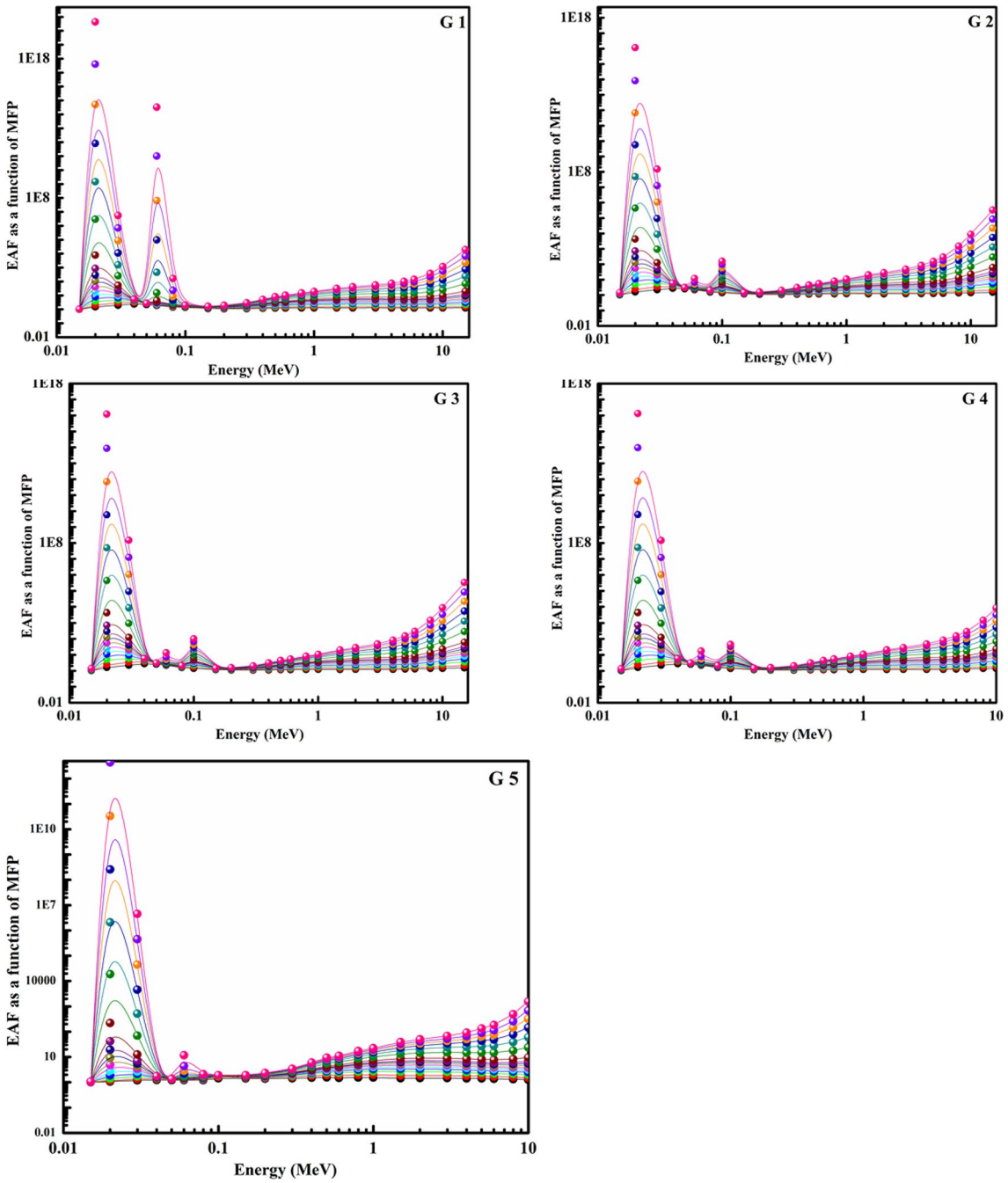

Fig. 13 EBF of fabricated samples

4 Conclusions

The melt quenching process was used for manufacturing glasses with a composition of $60SiO_2 - 35Pb_3O_4 - (5\text{-}x)$ ZnO-xY_2O_3 where ($0 \leq x \geq 5$) mol%. Amorphous character of the investigated samples was supported by the XRD, which demonstrated a total lack of observable crystalline peaks. The glass densities (ρ) increased from 5.91 gcm^{-3} for G1 to 6.97 gcm^{-3} for G5. Longitudinal velocity V_L increase from 4935 m/s to 5325 m/s, while transverse velocity V_T increase from 2520 m/s to 2905 m/s. Hardness improved from 4.41 to 8.31 GPa. With the addition of Y_2O_3 at varying mol%, the values of Young's modulus increment from 99.35 to 151.51 GPa, suggesting an increment in matrix stiffness. With successive additions of Y_2O_3, the bulk modulus similarly increased, rising from 93.89 to 119.21 GPa. The glasses' longitudinal modulus values (143.93–197.64 GPa) were higher than their corresponding shear modulus

G values (37.53–58.82 GPa) suggesting that they are more able to tolerate longitudinal stress than shear stress and that they are more easily bent than extended. The higher MAC values were produced by a decrease in ZnO concentration and an increase in Y_2O_3 content inside the glass matrix. As the concentration of Y_2O_3 increases, the MFP, TVL, and HVL values decrease. Better radiation shielding is provided by lower MFP, TVL, and HVL values. The MFP, TVL, and HVL values are lower in the G 5 sample with the Y_2O_3 contribution (5%, mole). Higher concentrations of Y_2O_3 in glasses with a SiO_2-Pb_3O_4-ZnO-composition were shown to have enhanced radiation shielding features. The data supplied indicates that the SiO_2-Pb_3O_4-ZnO-Y_2O_3 glass system is an effective absorber material that can be used in all industries where nuclear technologies are used.

Acknowledgements The authors express their gratitude to Princess Nourah bint Abdulrahman

University Researchers Supporting Project number (PNURSP2024R57), Princess Nourah bint Abdulrahman University, Riyadh, Saudi Arabia.

Author Contributions Kh. S. Shaaban, wrote the main manuscript text and prepared figures, Dalal Abdullah Aloraini, methodology, writing the manuscript, reviews the manuscript, E.A.Abdel Wahab methodology, writing the manuscript, reviews the manuscript, Ali S. Alzahrani, methodology, writing the manuscript, reviews the manuscript.

Funding None

Data Availability No datasets were generated or analysed during the current study.

Declarations

Ethics Approval and Consent to Participate The manuscript has not been published.

Consent to Participate and Publication The authors consent to participate and publish.

Informed Consent Not applicable.

Competing Interests The authors declare no competing interests.

References

1. Kurtulus R, Kavas T, Toplan HO, Akkurt I (2023) High-density and transparent boro-tellurite glass system against ionizing radiation: Fabrication and extensive characterization studies. Ceram Int 49, 11: Part B 18455–18462, https://doi.org/10.1016/j.ceramint.2023.02.217
2. Shaaban KS, Al-Baradi AM, Ali AM (2022) Gamma-ray shielding and mechanical characteristics of iron-doped lead phosphosilicate glasses. SILICON 14:8971–8979. https://doi.org/10.1007/s12633-022-01702-x
3. Aloraini DA, Ashour A, Shaaban KS (2023) Effect of Various Na_2O-MoO_3 Concentrations on the Thermal, Mechanical, and Radiation-resisting Attributes of Zinc-borosilicate Glasses. SILICON. https://doi.org/10.1007/s12633-023-02804-w
4. Rammah YS, El-Agawany FI, Wahab EAA, Hessien MM, Shaaban KS (2022) Significant impact of V_2O_5 content on lead phosphor-arsenate glasses for mechanical and radiation shielding applications. Radiat Phys Chem 193:109956. https://doi.org/10.1016/j.radphyschem.2021.109956
5. El-Maaref AA, Alotaibi BM, Alharbi N et al (2022) Effect of Fe_2O_3 as an Aggregate Replacement on Mechanical, and Gamma/Neutron Radiation Shielding Properties of Phosphoaluminate Glasses. J Inorg Organomet Polym 32:3117–3127. https://doi.org/10.1007/s10904-022-02345-6
6. Shaaban KS, Alotaibi BM, Alharbiy N et al (2022) Impact of TiO_2 on DTA and Elastic Moduli of Calcium Potassium Borophosphosilicate Glasses in Prelude for Use in Dental and Orthopedic Applications. SILICON 14:11991–12000. https://doi.org/10.1007/s12633-022-02029-3
7. Shaaban KS, Alyousef HA, Alotaibi BM et al (2022) The Vital Role of TiO_2 on the Bioglass System P2O5-CaO-B2O3-SiO2- K2O for Optics and Shielding Characteristics. J Inorg Organomet Polym 32:4295–4303. https://doi.org/10.1007/s10904-022-02446-2
8. Alghasham HA, Ismail YA, Aloraini DA, Shaaban K (2024) Elucidating the influences of MoO3 in Na2O- ZnO - B2O3 - SiO2: Fabrication, optical, and γ-ray protection properties for the novel high-density glasses. Materials Today Communications 38:107840. https://doi.org/10.1016/j.mtcomm.2023.107840
9. Koubisy MSI, Shaaban KS, Wahab EAA, Sayyed MI, Mahmoud KA (2021) Synthesis, structure, mechanical and radiation shielding features of $50SiO_2$–$(48+X)$ $Na_2B_4O_7$–$(2-X)$ MnO_2 glasses. Eur Phys J Plus 136 (2). https://doi.org/10.1140/epjp/s13360-021-01125-4.
10. Shaaban KS, Al-Baradi AM, Ali AM (2022) The Impact of Cr_2O_3 on the Mechanical, Physical, and Radiation Shielding Characteristics of $Na_2B_4O_7$–CaO–SiO_2 Glasses. SILICON 14:10375–10382. https://doi.org/10.1007/s12633-022-01783-8
11. Wahab EAA, Alyousef HA, El-Rehim AFA et al (2023) Basicity, Optical Features, and Neutron/Charged Particle Attenuation Characteristics of P2O5-As2O3-PbO Glasses Doped with Tungsten Ions. J Electron Mater 52:219–236. https://doi.org/10.1007/s11664-022-09969-x
12. Al-Baradi AM, Wahab EAA, Shaaban KS (2022) Preparation and Characteristics of B2O3 – SiO2 – Bi2O3 – TiO2 – Y2O3 Glasses and Glass-Ceramics. SILICON 14:5277–5287. https://doi.org/10.1007/s12633-021-01286-y
13. Althagafi TM, Sayed MA, Alghasham HA et al (2023) The Impact of Changing the LiF Concentration on Structural, Thermal, Physical, and Optical Properties of CdO—SiO_2—B_2O_3—MoO_3—LiF Glasses. SILICON. https://doi.org/10.1007/s12633-023-02567-4
14. Algarni SA, El-Maaref AA, Alotaibi BM et al (2022) Physical, Optical, and Radiation Shielding Features of Yttrium Lithium Borate Glasses. J Inorg Organomet Polym 32:2873–2881. https://doi.org/10.1007/s10904-022-02321-0
15. Shaaban KS, Al-Baradi AM, Ali AM (2022) Investigation of BaO reinforced TiO_2–P_2O_5–li_2O glasses for optical and neutron shielding applications. RSC Adv 12(5):3036–3043. https://doi.org/10.1039/d2ra00171c
16. Shaaban KhS, Tamam N, Hawra A, Alghasham ZA, Alrowaili MS, Al-Buriahi, Takwa E, Ellakwa (2023) Thermal, optical, and radiation shielding capacity of B_2O_3-MoO_3-Li_2O- Nb_2O_5 glasses. Mater Today Commun 37;107325. https://doi.org/10.1016/j.mtcomm.2023.107325
17. Shaaban KS, Alomairy S, Al-Buriahi MS (2021) Optical, thermal and radiation shielding properties of B_2O_3–NaF–PbO–BaO–La_2O_3 glasses. J Mater Sci: Mater Electron 32:26034–26048. https://doi.org/10.1007/s10854-021-05885-8

18. El-Rehim AFA, Zahran HY, Yahia IS, Wahab EAA, Shaaban KS (2021) Structural, Elastic Moduli, and Radiation Shielding of SiO_2-TiO_2-La_2O_3-Na_2O Glasses Containing Y_2O_3. J Mater Eng Perform 30:1872–1884. https://doi.org/10.1007/s11665-021-05513-w
19. Shaaban KS, Althagafi TM, Ashour A, Alalawi A, Al-Buriahi M, Ibraheem AA (2024) The role of Nb2O5 on structural, mechanical, and gamma-ray shielding characteristics of lithium molybdenum borate glasses. Radiat Phys Chem 216:111440. https://doi.org/10.1016/j.radphyschem.2023.111440
20. Sayyed MI, Sadeq MS, Kh S, Shaaban AF, El-Rehim A, Ali AM, Morshidy HY ((2023)) Elucidating the effect of La2O3–B2O3 exchange on structure, optical and radiation shielding improvements of Na2O–NiO–B2O3 glass. Opt Mater 142:114051. https://doi.org/10.1016/j.optmat.2023.114051
21. Sayed MA, Basha B, Al-Harbi N et al (2023) Investigation of Elastic Moduli and Gamma-Ray Shielding Parameters of P_2O_5-SiO_2-BaO Glasses Doped with Varying WO_3. SILICON 15:6463–6471. https://doi.org/10.1007/s12633-023-02537-w
22. Laifi J, Althagafi TM, Ibrahim EH et al (2023) Characterization of Mechanical and Radiation Shielding Ability of CdO - SiO_2 - B_2O_3 - MoO_3 - LiF Glasses. SILICON. https://doi.org/10.1007/s12633-023-02699-7
23. El-Rehim AFA, Shaaban KS (2021) Influence of La_2O_3 content on the structural, mechanical, and radiation-shielding properties of sodium fluoro lead barium borate glasses. J Mater Sci: Mater Electron 32:4651–4671. https://doi.org/10.1007/s10854-020-05204-7
24. B. Basha , Kh. S. Shaaban , E.A. Abdel Wahab (2023) The effect of tungsten ions on the structural, elastic moduli, and shielding characteristics of arsenic lead phosphate glasses. Dig J Nanomater Biostructures 18 (2):713 – 726. https://doi.org/10.15251/DJNB.2023.182.713
25. Shaaban KS, Alyousef HA, El-Rehim AFA (2022) CeO2 Reinforced B2O3–SiO2–MoO3 Glass System: A Characterization Study Through Physical, Mechanical and Gamma / Neutron Shields Characteristics. SILICON 14:12001–12012. https://doi.org/10.1007/s12633-022-02124-5
26. Şakar E, Özpolat ÖF, Alım B, Sayyed MI, Kurudirek M (2020) PhyX / PSD: Development of a user-friendly online software for calculation of parameters relevant to radiation shielding and dosimetry. Radiation Phys Chem 166:108496. https://doi.org/10.1016/j.radphyschem
27. Shaaban KS, Alotaibi BM, Algarni SA et al (2022) Chemical Composition, Mechanical, and Thermal Characteristics of Bioactive Glass for Better Processing Features. SILICON 14:10817–10826. https://doi.org/10.1007/s12633-022-01784-7
28. Shaaban KS, Al-Baradi AM, Wahab EAA (2022) The Impact of Y_2O_3 on Physical and Optical Characteristics, Polarizability, Optical Basicity, and Dispersion Parameters of B_2O_3 – SiO_2 – Bi_2O_3 – TiO_2 Glasses. SILICON 14:5057–5065. https://doi.org/10.1007/s12633-021-01309-8
29. Ali AM, Alrowaili ZA, Al-Baradi AM et al (2022) A Study of Thermal, and Optical Properties of $22SiO_2$-$23Bi_2O_3$-$37B_2O3$-$13TiO_2$-(5–x) LiF- x BaO Glasses. SILICON 14:6447–6455. https://doi.org/10.1007/s12633-021-01440-6
30. Shaaban KS, Alotaibi BM, Alharbiy N et al (2022) Fabrication of lithium borosilicate glasses containing Fe_2O_3 and ZnO for FT-IR, UV–Vis–NIR, DTA, and highly efficient shield. Appl Phys A 128:333. https://doi.org/10.1007/s00339-022-05474-4
31. Alomairy S, Aboraia AM, Shaaban ER, Shaaban KS (2021) Comparative Studies on Spectroscopic and Crystallization Properties of Al_2O_3 -Li_2O- B_2O_3-TiO_2 Glasses. Braz J Phys 51:1237–1248. https://doi.org/10.1007/s13538-021-00928-1
32. Alrowaili ZA, Al-Baradi AM, Sayed MA, Mossad Ali A, Abdel Wahab EA, Al-Buriahi MS, Shaaban KS (2021) The impact of Fe_2O_3 on the dispersion parameters and gamma / fast neutron shielding characteristics of lithium borosilicate glasses. Optik 168259. https://doi.org/10.1016/j.ijleo.2021.168259
33. Shaaban KS, Boukhris I, Kebaili I et al (2022) Spectroscopic and Attenuation Shielding Studies on B_2O_3-SiO_2-LiF- ZnO-TiO_2 Glasses. SILICON 14:3091–3100. https://doi.org/10.1007/s12633-021-01080-w
34. Sayyed MI, Morshidy HY, Shaaban KhS, Abd El-Rehim AF, Ali AM, Sadeq MS (2023) Impacts of BaO additions on structure, linear/nonlinear optical properties and radiation shielding competence of BaO–NiO–ZnO–B2O3 glasses. Opt Mater 144:114300. https://doi.org/10.1016/j.optmat.2023.114300
35. Wahab EAA, Ahmed EM, Rammah YS et al (2022) Basicity, Electronegativity, Optical Parameters and Radiation Attenuation Characteristics of P_2O_5-As_2O_3-PbO Glasses Doped Vanadium Ions. J Inorg Organomet Polym 32:3983–3996. https://doi.org/10.1007/s10904-022-02400-2
36. Alrowaili ZA, Ali AM, Al-Baradi AM et al (2022) A significant role of MoO_3 on the optical, thermal, and radiation shielding characteristics of B_2O_3–P_2O_5–Li_2O glasses. Opt Quant Electron 54:88. https://doi.org/10.1007/s11082-021-03447-0
37. Shaaban KhS, Alotaibi BM, Alharbi N, Alrowaili ZA, Al-Buriahi MS, Sayed AM, Abd El-Rehim AF (2022) Physical, optical, and radiation characteristics of bioactive glasses for dental prosthetics and orthopaedic implants applications. Radiat Phys Chem 193:109995. https://doi.org/10.1016/j.radphyschem.2022.109995.
38. Shaaban KS, Al-Baradi AM, Ali AM (2022) Physical, optical, and advanced radiation absorption characteristics of cadmium lead phosphate glasses containing MoO_3. J Mater Sci: Mater Electron 33:3297–3305. https://doi.org/10.1007/s10854-021-07530-w
39. Alomairy S, Alrowaili ZA, Kebaili I et al (2022) Synthesis of Pb_3O_4-SiO_2-ZnO-WO_3 Glasses and their Fundamental Properties for Gamma Shielding Applications. SILICON 14:5661–5671. https://doi.org/10.1007/s12633-021-01347-2
40. Mahmoud K, Alsubaie A, Wahab EAA et al (2022) Research on the Effects of Yttrium on Bismuth Titanate Borosilicate Glass System. SILICON 14:3419–3427. https://doi.org/10.1007/s12633-021-01125-0
41. Shaaban KhS, Al-Baradi AM, Alotaibi BM, Abd El-Rehim AF (2023) Mechanical and radiation shielding features of lithium titanophosphate glasses doped BaO, J Mater Res Technol 23, 756–764. https://doi.org/10.1016/j.jmrt.2023.01.062
42. Shaaban KS, Alotaibi BM, Alrowaili ZA et al (2023) Thermal and Mechanical Studies of Cerium Molybdenum Borosilicate Glasses and Glass-Ceramics. SILICON 15:5233–5243. https://doi.org/10.1007/s12633-023-02433-3
43. Shaaban KS, Alrowaili ZA, Al-Baradi AM et al (2022) Mechanical and Thermodynamic Characteristics of $22SiO_2$-$23Bi_2O_3$-$37B_2O3$-$13TiO_2$-(5–x) LiF- x BaO Glasses. SILICON 14:6457–6465. https://doi.org/10.1007/s12633-021-01441-5
44. Al-Baradi AM, Alotaibi BM, Alharbi N et al (2022) Gamma Radiation Shielding and Mechanical Studies on Highly Dense Lithium Iron Borosilicate Glasses Modified by Zinc Oxide. SILICON 14:10391–10399. https://doi.org/10.1007/s12633-022-01801-9
45. Almuqrin AH, Mahmoud KA, Wahab EAA, Koubisy MSI, Sayyed MI, Shaaban KS (2021) Structural, mechanical, and nuclear radiation shielding properties of iron aluminoleadborate glasses. Eur Phys J Plus 136 (6). https://doi.org/10.1140/epjp/s13360-021-01564-z
46. Alothman MA, Alrowaili ZA, Alzahrani JS, Wahab EAA, Olarinoye IO, Sriwunkum C, Shaaban KS, Al-Buriahi MS (2021) Significant influence of MoO_3 content on synthesis, mechanical, and radiation shielding properties of B_2O_3-Pb_3O_4-Al_2O_3 glasses. J Alloy Compd 882:160625. https://doi.org/10.1016/j.jallcom.2021.160625

47. Shaaban KS, Basha B, Alrowaili ZA, Al-Buriahi MS, Abdel Wahab EA (2023) A closer inspection of the structural, mechanical, optical and radiation shielding properties of GeO2-doped magnesium-telluroborate glasses. Radiochim Acta 111(9):713–724. https://doi.org/10.1515/ract-2023-0140
48. Arun K (1994) Varshneya, Fundamentals of Inorganic Glasses, Gulf Professional Publishing P,33
49. Makishima A, Mackenzie JD (1975) Calculation of bulk modulus, shear modulus and Poisson's ratio of glass. J Non-Cryst Solids 17(2):147–157. https://doi.org/10.1016/0022-3093(75)90047-2
50. Makishima A, Mackenzie JD (1973) Direct calculation of Young's moidulus of glass. J Non-Cryst Solids 12(1):35–45. https://doi.org/10.1016/0022-3093(73)90053-7
51. Al-Baradi AM, El-Rehim AFA, Alrowaili ZA, Al-Buriahi MS, Shaaban KS (2021) FT-IR and Gamma Shielding Characteristics of $22SiO_2$- $23Bi_2O_3$-$37B_2O_3$-$13TiO_2$-(5–x) LiF- x BaO Glasses. SILICON 14(12):7043–7051. https://doi.org/10.1007/s12633-021-01481-x
52. Wahab EAA, Al-Baradi AM, Sayed MA et al (2022) Crystallization and Radiation Proficiency of Transparent Sodium Silicate Glass Doped Zirconia. SILICON 14:8581–8597. https://doi.org/10.1007/s12633-021-01652-w
53. Sayed MA, Basha B, Al-Harbi N et al (2023) PbO effect on physical, mechanical, optical, structural, and radiation characteristics of P_2O_5-BaO-PbO glass system. Eur Phys J Plus 138:455. https://doi.org/10.1140/epjp/s13360-023-04079-x
54. El-Taher A, Zakaly HMH, Pyshkina M, Allam EA, El-Sharkawy RM, Mahmoud ME, Abdel-Rahman MAE (2021) A comparative Study Between Fluka and Microshield Modeling Calculations to study the Radiation-Shielding of Nanoparticles and Plastic Waste composites, Zeitschrift Fur Anorg. Und Allg. Chemie 647:1083–1090. https://doi.org/10.1002/zaac.202100062
55. Henaish AMA, Mostafa M, Salem BI, Zakaly HMH, Issa SAM, Weinstein IA, Hemeda OM (2020) Spectral, electrical, magnetic and radiation shielding studies of Mg-doped Ni–Cu–Zn nanoferrites. J Mater Sci Mater Electron 31:20210–20222. https://doi.org/10.1007/s10854-020-04541-x
56. Zakaly HMH, Uosif MAM, Issa SAM, Tekin HO, Madkour H, Tammam M, El-Taher A, Alharshan GA, Mostafa MYA (2021) An extended assessment of natural radioactivity in the sediments of the mid-region of the Egyptian Red Sea coast. Mar Pollut Bull 171:112658. https://doi.org/10.1016/J.MARPOLBUL.2021.112658
57. Tekin HO, Issa SAM, Kilic G, Zakaly HMH, Tarhan N, Sidek HAA, Matori KA, Zaid MHM (2021) A systematical characterization of teo2–v2o5 glass system using boron (Iii) oxide and neodymium (iii) oxide substitution: Resistance behaviors against ionizing radiation. Appl Sci 11:3035. https://doi.org/10.3390/app11073035
58. Almisned G, Elshami W, Issa SAM, Susoy G, Zakaly HMH, Algethami M, Rammah YS, Ene A, Al-Ghamdi SA, Ibraheem AA, Tekin HO (2021) Enhancement of gamma-ray shielding properties in cobalt-doped heavy metal borate glasses: The role of lanthanum oxide reinforcement. Materials (Basel) 14:7703. https://doi.org/10.3390/ma14247703
59. Zakaly HMH, Issa SAM, Tekin HO, Badawi A, Saudi HA, Henaish AMA, Rammah YS (2022) An experimental evaluation of CdO/PbO-B2O3 glasses containing neodymium oxide: Structure, electrical conductivity, and gamma-ray resistance. Mater Res Bull 111828.https://doi.org/10.1016/j.materresbull.2022.111828
60. Tekin HO, ALMisned G, Zakaly HMH, Zamil A, Khoucheich D, Bilal G, Al-Sammarraie L, Issa SAM, Al-Buriahi MS, Ene A (2022) Gamma, neutron, and heavy charged ion shielding properties of Er3+-doped and Sm3+-doped zinc borate glasses. Open Chem 20 130–145.https://doi.org/10.1515/CHEM-2022-0128
61. Zakaly HM, Abouhaswa AS, Issa SAM, Mostafa MYA, Pyshkina M, El-Mallawany R (2020) Optical and nuclear radiation shielding properties of zinc borate glasses doped with lanthanum oxide. J Non Cryst Solids 543:120151. https://doi.org/10.1016/j.jnoncrysol.2020.120151
62. Zakaly HMH, Issa SAM, Saudi HA, Alharshan GA, Uosif MAM, Henaish AMA (2022) Structure, Mössbauer, electrical, and γ-ray attenuation-properties of magnesium zinc ferrite synthesized co-precipitation method. Sci Rep 12:1–16. https://doi.org/10.1038/s41598-022-17311-y
63. Kaky KM, Sayyed M, Khammas A, Kumar A, Şakar E, Abdalsalam AH, Cevïz Şakar, B., Alim, B., & Mhareb, M. (2020) Theoretical and experimental validation gamma shielding properties of B2O3–ZnO–MgO–Bi2O3 glass system. Mater Chem Phys 242:122504. https://doi.org/10.1016/j.matchemphys.2019.122504
64. Lakshminarayana G, Sayyed MI, Baki SO et al (2018) Optical absorption and gamma-radiation-shielding parameter studies of Tm^{3+}-doped multicomponent borosilicate glasses. Appl Phys A 124:378. https://doi.org/10.1007/s00339-018-1801-4
65. Kaky KM, Şakar E, Akbaba U, Emre Kasapoğlu A, Sayyed M, Gür E, Baki S, Mahdi M (2019) X-ray photoelectron spectroscopy (XPS) and gamma-ray shielding investigation of boro-silicate glasses contained alkali/alkaline modifier. Results in Physics 14:102438. https://doi.org/10.1016/j.rinp.2019.102438
66. Mhareb M, Alqahtani M, Alajerami Y, Alshahri F, Sayyed M, Mahmoud K, Saleh N, Alonizan N, Al-Buriahi M, Kaky KM (2021) Ionizing radiation shielding features for titanium borosilicate glass modified with different concentrations of barium oxide. Mater Chem Phys 272:125047. https://doi.org/10.1016/j.matchemphys.2021.125047
67. Hassib MD, Kaky KM, Kumar A, Şakar E, Sayyed M, Baki S, Mahdi M (2019) Boro-silicate glasses co-doped Er+3/Yb+3 for optical amplifier and gamma radiation shielding applications. Physica B 567:37–44. https://doi.org/10.1016/j.physb.2019.05.006
68. Kaky, Kawa M. Lakshminarayana G, Baki SO, Halimah MK, Mahdi M A (2017) Structural, thermal and optical studies of bismuth doped multicomponent tellurite glass. Solid State Phenomena 268: 165-171. ISSN 1012–0394; ESSN: 1662–9779. https://doi.org/10.4028/www.scientific.net/SSP.268.165
69. Lakshminarayana G, Kaky KM, Jedryka J, El-Naggar A, Albassam A, Myronchuk G, Mahdi M (2016) Laser induced elastooptics in novel Bi2O3, and Pr2O3 doped tellurite rich glasses. Mater Lett 183:322–324. https://doi.org/10.1016/j.matlet.2016.07.129
70. Kaky KM, Sayyed M (2024) Selected germanate glass systems with robust physical features for radiation protection material use. Radiat Phys Chem 215:111321. https://doi.org/10.1016/j.radphyschem.2023.111321
71. Kaky KM, Sayyed M, Mhareb M, Abbas HH, Baki S (2023) Physical, structural, mechanical, and various radiation shielding properties of TeO2-GeO2-ZnO-Al2O3-Li2O-M (M= WO3, MoO3, PbO, and CuO) glasses. Opt Mater 145:114370